

# The possible detection of high redshift Type II QSOs in deep fields

Avery Meiksin

*SUPA\**, *Institute for Astronomy, University of Edinburgh, Blackford Hill, Edinburgh EH9 3HJ, UK*

10 June 2021

## ABSTRACT

The colours of high redshift Type II QSOs are synthesized from observations of moderate redshift systems. It is shown that Type II QSOs are comparable to starbursts at matching the colours of  $z_{850}$ -dropouts and  $i_{775}$ -drops in the Hubble Ultra Deep Field, and more naturally account for the bluest objects detected. Type II QSOs may also account for some of the  $i_{775}$ -drops detected in the GOODS fields. It is shown that by combining imaging data from the *Hubble Space Telescope* and the *James Webb Space Telescope*, it will be possible to clearly separate Type II QSOs from Type I QSOs and starbursts based on their colours. Similarly, it is shown that the UKIDSS *ZYJ* filters may be used to discriminate high redshift Type II QSOs from other objects. If Type II QSOs are prevalent at high redshifts, then AGN may be major contributors to the re-ionization of the Intergalactic Medium.

**Key words:** galaxies: active - galaxies: high redshift - galaxies: starburst - quasars: emission lines - quasars: general - surveys

## 1 INTRODUCTION

The band-dropout method has proven an impressive means for discovering high redshift objects. Pioneered by Guhathakurta et al. (1990), Bithell (1991), and Steidel & Hamilton (1992, 1993), the method exploits the downward step in flux shortward of the Lyman limit for discovering starburst galaxies. Absorption by intervening hydrogen in the Intergalactic Medium (IGM) will similarly produce extremely red optical colours for objects at  $z \gtrsim 3$ , a characteristic signature of a high redshift system (Bithell 1991; Madau 1995). Following Steidel & Hamilton’s discovery of a population of Lyman break galaxies at  $z \approx 3$ , the method has evolved into a standard tool for identifying even higher redshift objects in recent very deep surveys like the Hubble Deep Field and the Ultra-Deep Field. While follow-up spectroscopy has demonstrated that most of the objects are galaxies, a few dozen reveal the emission line signatures of Active Galactic Nuclei (AGN) (Steidel et al. 2002), about half of which have the narrow lines characteristic of Type II systems. These AGN have made possible the first measurement of the faint end of the luminosity function of Quasi-Stellar Objects (QSOs) at  $z \approx 3$  (Hunt et al. 2004), critical for assessing the poorly constrained contribution of QSOs to the UV ionizing background at this epoch (Meiksin 2005a).

Since then, band-dropout objects have been discovered

in a host of surveys, most recently pushing to  $z \approx 6$  (Stanway, Bunker & McMahon 2003; Bouwens et al. 2004; Bunker et al. 2004; Yan & Windhorst 2004; Giavalisco et al. 2004). The objects have generally been modelled as young star-forming galaxies and used to infer the cosmic star formation rate of the universe and its evolution. They have also been used to assess the contribution of galaxies to the budget of ionizing photons required to re-ionize the universe, concluding their numbers are either too few (Bunker et al. 2004) or easily adequate (Stiavelli et al. 2004), depending on model assumptions.

In this paper, it is suggested that a portion of the band-dropout objects may be Type II QSOs.<sup>†</sup> The prospects of detecting Type II QSOs in deep surveys has not previously been explored. These objects have been of considerable recent interest because they are predicted in unification models of AGN (Antonucci 1993). Discovering examples at higher redshifts would help to further elucidate their properties and their connection to Type I QSOs. As sources of energetic photons, they are also candidate sources for high

<sup>†</sup> There is not universal consensus on the definition of a Type II QSO. In this paper, a definition similar to that of Zakamska et al. (2003) is assumed, that the restframe FWHM of hydrogen lines be less than  $2000 \text{ km s}^{-1}$ . An alternative x-ray motivated definition is based on x-ray spectral evidence for a large obscuring H I column density local to the active nucleus, for example, Gandhi et al. (2004).

\* Scottish Universities Physics Alliance

energy background radiations. Obscured QSOs have been postulated as sources of the hard x-ray background (Madau, Ghisellini & Fabian 1994), and Type II QSOs are natural candidates for such sources. While Type I QSOs may dominate the UV ionizing metagalactic background at  $z \lesssim 3.5$ , their numbers appear inadequate at higher redshifts (eg, Meiksin 2005a). Although galaxies are possible sources, the abundance of high redshift Type II QSOs is far too uncertain to rule out an ionizing background dominated by AGN sources. If their numbers are sufficiently great at high redshifts, Type II QSOs may also have contributed substantially to the re-ionization of the IGM. Indeed, if the IGM were re-ionized at  $z = 6 - 8$ , consistency with measurements of the optical depth of the IGM at  $z < 6$  favour hard ionizing sources like Pop III stars and AGN (Meiksin 2005a).

The Sloan Digital Sky Survey (SDSS) has discovered nearly 300 Type II QSOs over the redshift range  $0.3 < z < 0.83$ , with the rest wavelengths of the measured spectra restricted to being longward of about 2100 Å (Zakamska et al. 2003). These elusive narrow-lined objects have proven even more difficult to discover at higher redshifts, and their UV spectral properties are consequently still poorly understood. To date, only four Type II QSOs are known to exist at  $z > 1.5$  with optical spectra showing narrow emission lines, two discovered through observations with the *Chandra X-Ray Observatory* (Norman et al. 2002; Mainieri et al. 2005), one discovered as an optical band-dropout (Stern et al. 2002), and one discovered through optical spectroscopy (Jarvis et al. 2005). A fifth candidate was found by Dawson et al (2001), but with incomplete emission line results reported. The discovery of high redshift counterparts would add substantially to our knowledge of the nature and origin of these systems.

## 2 SOURCE MODELS

To more clearly delineate the differences between the predicted colours of Type II QSOs and other possible sources, the colours of starburst galaxies and Type I QSOs are also considered. Stanway, McMahon & Bunker (2005) previously considered starbursts as the origin of their  $i_{775}$ -drops found in the Hubble Ultra-Deep Field (UDF), and found they were unable to match the colours of the bluest sources in  $(J_{110} - H_{160})_{AB}$ , including a population of blue sources too dim to measure in  $J_{110}$  but for which colours are inferred from image stacking. Their results are confirmed and slightly extended here. Bouwens et al. discovered  $z_{850}$ -dropouts in the UDF with similarly blue  $(J_{110} - H_{160})_{AB}$  colours. The  $i_{775}$ -drops detected in the UDF by Bunker et al. (2004) and Yan & Windhorst (2004) are also considered, as are the  $i_{775}$ -drops reported by Stanway, Bunker & McMahon (2003) and Eyles et al. (2005) as part of the Great Observatories Origins Deep Survey (GOODS).

The starbursts models used here were generated using the STARBURST99 package of Leitherer et al. (1999). Continuous star formation is assumed with a Salpeter Initial Mass Function. Nebular emission lines are included. Solar metallicity is assumed, although the colour results below are not very sensitive to the metallicity. For instance, using a metallicity of 0.05 solar reduces  $(z_{850} - J_{110})_{AB}$  for a 30 Myr starburst at  $z \approx 6$  by less than 0.01 mag below

the value for solar metallicity and  $(J_{110} - H_{160})_{AB}$  by less than 0.1 mag. Colours are presented in the figures below for ages of 30 Myr and 600 Myr, which is just under the age of the universe at  $z \approx 8.5$  for a cosmology with  $\Omega_M = 0.3$ ,  $\Omega_v = 0.7$ , and  $h = 0.7$ .

The Type I QSO spectrum adopted is the median spectrum constructed by Vanden Berk et al. (2001) from the SDSS QSO survey. It is a composite of over 2200 spectra homogeneously selected from the SDSS QSO survey covering the redshift range  $0.044 \leq z \leq 4.789$ . The spectrum covers the rest wavelength range 800 – 8555 Å. While the colours of Type I QSOs will show a fairly wide spread, as investigated by Chiu et al. (2005), the median composite is a good indicator of the locus of a Type I QSO in colour space.

Since no flux-calibrated spectra of Type II QSOs exist that clearly reveal the continuum over an extended wavelength range, a Type II prototype spectrum is constructed from measured broad band magnitudes and emission lines. In addition to having narrower emission lines, there is an indication in the literature that some Type II QSOs differ from Type I QSOs in another fundamental aspect: several of the emission lines appear often to have high equivalent widths comparable to the filter bandwidths. This will give them unusual colours, especially at high redshifts, since the emission lines will dominate the continuum light in a given passband. It is the observational consequences of this particular feature of some Type II QSOs that is emphasized in this paper, although low equivalent width Type II QSOs are also considered.

Estimating the contribution of the emission lines to the Type II QSO colours, however, has several uncertainties. The spectra and photometry are measured through different size apertures. This requires an aperture correction for which an arbitrary assumption must be made regarding any possible spatial variation of the light in the emitting regions. Norman et al. show substantial corrections to the measured magnitudes of a Type II QSO after removing the emission lines. Unfortunately they do not indicate the size of the aperture correction they must have used. The weaknesses of the reported flux values of the emission lines compared with the broadband-integrated fluxes show, however, that an aperture correction of  $\sim 20$  must have been applied, which seems rather high. The Mainieri et al. QSO has low equivalent width emission lines, so that its spectrum will differ little from that of an AGN-hosting ULIRG like NGC 6240 when boosted to higher redshifts, which well matches the colours measured by Mainieri et al. The Jarvis et al. QSO is at too low a redshift to detect Ly $\alpha$ .

Only the Stern et al. QSO, CXO 52 ( $z = 3.288$ ) provides all the requirements for constructing a Type II QSO spectrum in the UV with high equivalent width emission lines. The emission line properties they fit are shown in Table 1. It should be noted that the published Table 2 in Stern et al. contains a misprint in the column heading for the equivalent widths, mistakenly indicating they are in the rest frame when in fact they are in the observer's frame (D. Stern personal communication). The emission lines were measured from a spectrum taken through a 1.5" x 1.5" aperture. The magnitudes reported are for a 3" diameter aperture. Without detailed surface brightness profiles of the continuum and emission line emitting regions, it is not possible to make

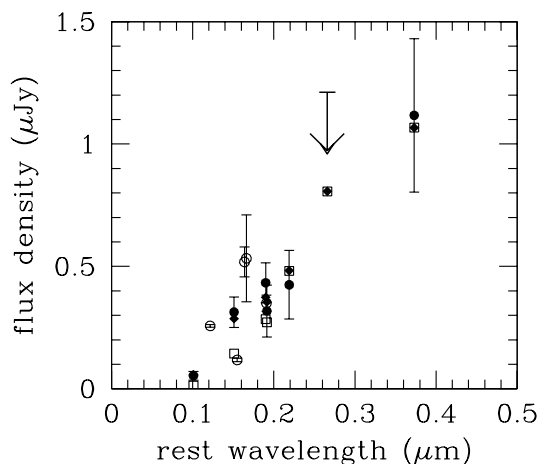


**Figure 1.** The measured and synthesized flux densities for the Type II QSO CXO 52. The measured flux densities in each band from Stern et al. (2002) are shown by the filled points with error bars, and one upper limit. The wavelengths are in the rest frame of the QSO. The inferred un-attenuated continuum of the QSO is shown by the open squares. The predicted flux densities, including the contribution from the emission lines and the effect of intergalactic attenuation, are shown by the filled diamonds. The open points with error bars show the aperture-corrected continuum levels inferred from the measured fluxes and equivalent widths of the optical emission lines reported by Stern et al.

Line	Flux ( $10^{-17}$ ergs $\text{cm}^{-2}$ $\text{s}^{-1}$ )	$W_\lambda$ (obs) ( $\text{\AA}$ )	$W_\lambda^{\text{a.c.}}$ (obs) ( $\text{\AA}$ )
O VI $\lambda$ 1035	1.5:	120:	345
Ly $\alpha$	$18.9 \pm 0.4$	$2100 \pm 40$	1948
N V $\lambda$ 1240	0.6:	50:	56
Si IV /O IV ] $\lambda$ 1403	0.4:	30:	20
C IV $\lambda$ 1549	$3.5 \pm 0.2$	$350 \pm 20$	676
He II $\lambda$ 1640	$1.7 \pm 0.2$	$170 \pm 20$	361
O III $\lambda$ 1663	$0.9 \pm 0.3$	$90 \pm 30$	196
C III ] $\lambda$ 1909	$2.1 \pm 0.2$	$420 \pm 40$	574

**Table 1.** Emission line measurements of CXO 52 from Stern et al. (2002). The first equivalent width column is as measured through a  $1.5'' \times 1.5''$  aperture; the second column is aperture-corrected to a  $3''$  diameter aperture (see text). Parameters with colons indicate uncertain measurements. The equivalent width values are in the observer's frame.

an assumption-free comparison of the overall contribution of the emission lines to the broadband fluxes. In particular, the optical broadband flux densities in Table 1 of Stern et al. indicate flux levels of about  $0.3 \mu\text{Jy}$ , while the optical spectrum in their Figure 3 shows a continuum level of about  $0.1 \mu\text{Jy}$ . Except possibly for Ly $\alpha$ , the quoted equivalent widths in their Table 2 are too small for the emis-

sion lines to dominate the broadband optical magnitudes, so that the difference in the broadband and spectral continuum flux levels indicates that the continuum extends beyond the  $1.5'' \times 1.5''$  slit. It is consequently necessary to make some assumptions regarding the spatial distribution of the emission line and continuum emitting regions to infer the contribution of the emission lines to the broadband colours.

The Ly $\alpha$  emitting region in Figure 5 of Stern et al. clearly extends beyond the  $1.5'' \times 1.5''$  aperture. Although the emission-line region may peak within the  $1.5'' \times 1.5''$  aperture, its surface brightness distribution is unknown. If shallow, it is still possible that the integrated flux of the emission-line region continues to increase substantially beyond the slit. The assumption adopted here is that the line-emitting region fills the  $3''$  aperture used for the broadband magnitudes, and an aperture correction is applied assuming uniform surface brightness.

The aperture-corrected emission line fluxes are then removed from the broadband magnitude measurements to infer the levels of the underlying continuum. The spectrum is then constructed by fitting power-laws between the values of the continuum at the effective wavelengths of each filter, adjusting the values to match the measured magnitudes after re-introducing the emission lines. Because some of the magnitude measurements correspond to rest wavelengths shortward of Ly $\alpha$ , the spectrum is corrected for IGM absorption using the values from Meiksin (2005b). The shortest wavelengths are synthesized by extending the UV portion of the spectrum to the x-ray using the measured *Chandra* flux in the 0.5 – 2 keV band (Stern et al. ). The intrinsic and predicted magnitudes, including IGM attenuation, are compared with those measured in Figure 1. Also shown are the continuum levels inferred from the measured fluxes and equivalent widths of the optical emission lines reported by Stern et al. The continuum levels are shown at the line centres and corrected to a  $3''$  aperture. Agreement with the continuum levels inferred from the emission-line subtracted broadband fluxes is good, although the emission line-inferred continuum levels are somewhat high near rest-frame  $\lambda \approx 0.16 \mu\text{m}$ .

In terms of the relative contribution of the emission lines to the continuum, the above procedure is equivalent to assuming a constant surface brightness for the continuum, aperture-corrected downwards to the  $1.5'' \times 1.5''$  spectroscopic slit, although this would then require the corresponding correction be applied to the quoted total broadband magnitudes. It should be clear that the total magnitudes being presented here are based on apertures that are filled by the emission-line emitting regions. Should the continuum extend well beyond the emission line regions, then magnitudes measured through apertures larger than the emission-line regions will be more weighted toward the continuum. As the apertures used for broadband optical magnitude measurements with *HST* typically have diameters of  $0.5''$ – $1.0''$ , this is not generally expected to be a major complication, although it will obviously depend on the properties of each source.

The H $\alpha$  and O III  $\lambda\lambda$ 4959, 5007 lines detected by Stern et al. lie within the  $K_s$  band for the QSO. These lines, after aperture-correcting, are, within the errors, able to account fully for the measured  $K_s$  magnitude. It is consequently not possible to make a firm continuum estimate for the QSO at

these wavelengths, nor a reliable estimate for the aperture-corrected equivalent widths of these lines. Although  $K_s$  predictions are made below at higher redshifts, these predictions are quite uncertain for  $z \lesssim 4$ , being based almost entirely on the aperture-corrected fluxes of these three lines. Since the longest wavelength near-infra-red continuum point that is firmly established is based on observations through the  $F160W$  filter, the  $K_s$  predictions are in fact fairly uncertain up to  $z \lesssim 5.3$ .

The equivalent widths inferred for the emission lines in a  $3''$  aperture are provided in Table 1. It should be noted that while the equivalent widths are similar to those reported by Stern et al., a few are larger. This may be a consequence of the aperture correction applied to the emission lines. Under the alternative view of aperture correcting the broadband continuum magnitudes from the  $3''$  diameter aperture to the  $1.5'' \times 1.5''$  slit, the equivalent widths would be expected to be the same. It is possible that the equivalent width errors quoted in Table 2 of Stern et al. are underestimates, as they appear only to account for the errors in the measured emission line fluxes, not for the errors in the fit continuum levels. The spectrum shown in their Figure 3 suggests the continuum is comparable to the noise level, so that the continuum error may be large. In any case, the purpose here is not to provide a definitive spectrum, but a plausible one consistent with the data. The effect of varying the strengths of the emission lines on the predicted colours will be considered below to allow for the uncertainty in their equivalent widths, as well as possible source metallicity variations.

As a contrast to CXO 52, a spectrum for the Type II QSO CDFS-263 at  $z = 3.660$  with low equivalent width emission lines discovered by Mainieri et al. is also synthesized, using exactly the same procedure as for CXO 52. This spectrum will be referred to as the “low equivalent width” Type II QSO; otherwise colours based on CXO 52 are generally meant when referring to Type II QSOs.

### 3 HIGH REDSHIFT COLOUR PREDICTIONS

#### 3.1 Comparison with Ultra-Deep Field

##### $z_{850}$ -dropouts

The evolution of the predicted  $(i_{775} - z_{850})_{AB}$ ,  $(z_{850} - J_{110})_{AB}$  and  $(J_{110} - H_{160})_{AB}$  colours of the candidate sources are shown in Figure 2. The entrance of the  $\text{Ly}\alpha$  emission line of the high equivalent width Type II QSO into the  $z_{850}$  passband (middle panel) is visible as a sharp blueing for  $z \gtrsim 5.7$ . The object becomes a  $z_{850}$ -dropout quite abruptly at  $z > 7.6$ , at which point it is the bluest of the candidate sources in  $(J_{110} - H_{160})_{AB}$ .

Bouwens et al. (2004) detect four  $z_{850}$ -dropouts in the Hubble Ultra-Deep Field, interpreting them as starbursts in the redshift range  $7 < z < 8$ , to which the  $z_{850}$ -dropout method is sensitive through the detection of the  $\text{Ly}\alpha$  break. These objects are unusually blue in  $(J_{110} - H_{160})_{AB}$ , bluer than predicted for starbursts starbursts, even when the light is dominated by Pop III objects. To model the colours, the ACS  $F850LP$  filter transmission is combined with the total quantum efficiency of the detector to compute  $z_{850}$ . Similarly, the NICMOS  $F110W$  and  $F160W$  filters are used to compute  $J_{110}$  and  $H_{160}$ . The AB scale is assumed throughout. The effects of intergalactic attenuation are included

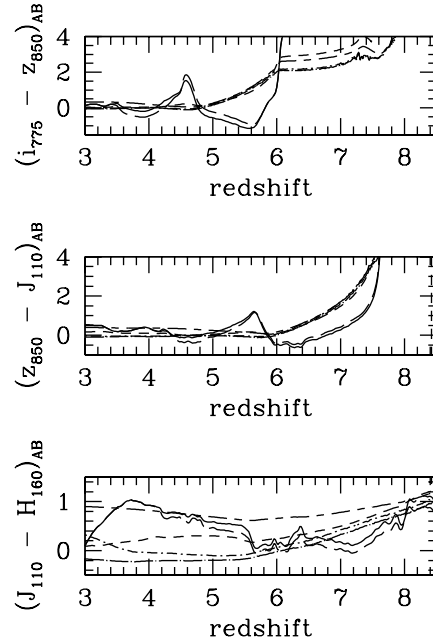


**Figure 2.** The redshift evolution of  $(i_{775} - z_{850})_{AB}$ ,  $(z_{850} - J_{110})_{AB}$  and  $(J_{110} - H_{160})_{AB}$  colours predicted for starburst galaxies of age 30 Myr (dotted long-dashed lines) and 600 Myr (dotted short-dashed lines), Type I QSO (short-dashed lines), and high equivalent width Type II QSO (solid lines). The long-dashed line shows the track for the Type II QSO with C IV enhanced by a factor of 2. The blueing in  $(i_{775} - z_{850})_{AB}$  for the Type II QSO at  $z > 4.6$  is due to the entering of the  $\text{Ly}\alpha$  emission line into the  $i_{775}$  passband, which it then leaves by  $z \gtrsim 6$ . Similarly, the blueing in  $(z_{850} - J_{110})_{AB}$  for the Type II QSO at  $z > 5.7$  is due to the entering of the  $\text{Ly}\alpha$  emission line into the  $z_{850}$  passband, which it then leaves by  $z = 7.6$ . The short-dashed long-dashed lines show the results for a low equivalent width Type II QSO.

(Meiksin 2005b). The  $(z_{850} - J_{110})_{AB}$  vs  $(J_{110} - H_{160})_{AB}$  colours are shown for the two starburst models and the Type I and Type II QSO spectra in Figure 3. The Type I QSO, the low equivalent width Type II QSO and the 600 Myr starburst galaxy colours poorly match the  $z_{850}$ -dropout colours. The large equivalent width Type II QSO and 30 Myr starburst are equally good matches.

Because of the uncertain equivalent widths of the metal emission lines in CXO 52, the effect of varying them is explored. This may also be considered a change in the overall metallicity, although it ignores any effect changing the metallicity may have on the thermodynamics of the emitting gas and hence the emission line strengths. For  $(z_{850} - J_{110})_{AB} < 1.8$ , boosting the metallicity by 50% renders the Type II QSO bluer in  $(J_{110} - H_{160})_{AB}$ , while it is reddened for  $(z_{850} - J_{110})_{AB} > 1.8$ . Decreasing the metallicity by 50% has the opposite effect. The effect on the  $z_{850}$ -dropouts is small, as shown in Figure 3.

The emission line flux ratios for CXO 52 are consistent with the photoionization models presented in Table 6

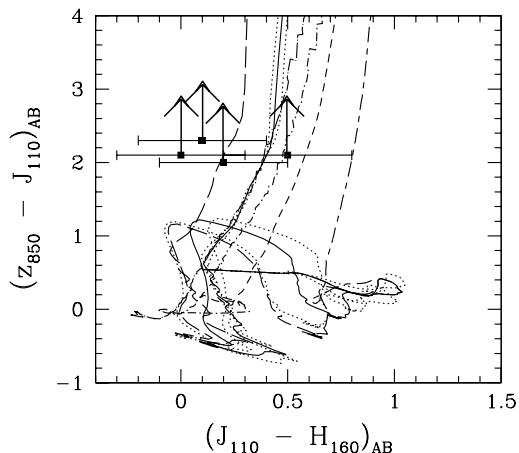


**Figure 3.**  $(z_{850} - J_{110})_{AB}$  vs  $(J_{110} - H_{160})_{AB}$  colour-colour diagram showing the position of the  $z_{850}$ -dropouts of Bouwens et al. and the predicted tracks at  $z > 3$  for starburst galaxies of age 30 Myr (dotted long-dashed line) and 600 Myr (dotted short-dashed line), Type I QSO (short-dashed line), and Type II QSO with high equivalent width emission lines (solid line). The dotted lines show the tracks for the Type II QSO with the metal lines boosted or reduced by 50%. The long-dashed line shows the track for the Type II QSO with C IV enhanced by a factor of 2. The short-dashed long-dashed line shows the predictions for a low equivalent width Type II QSO.

of Kwan & Krolik (1981) for clouds exposed to an AGN spectrum. These models predict that most of the carbon is in the form of C II, and that increasing the density of the clouds tends to increase the emission ratio of C IV  $\lambda 1549$  to C III  $\lambda 1909$ . A model with the C IV equivalent width doubled, holding all else fixed, is shown in Figure 3. The colour track now runs through the  $z_{850}$ -dropout points. Although it is not possible to rule out statistically the possibility that all four objects are starbursts, this does show that Type II QSOs are plausible candidates. In particular, the three bluest objects, taken collectively with an average  $(J_{110} - H_{160})_{AB} \approx 0.1 \pm 0.2$ , are consistent with a 30 Myr starburst and 600 Myr starburst only at the  $1.5\sigma$  and  $2\sigma$  levels, respectively, favouring the interpretation that one or more of these three is a Type II QSO with large equivalent widths.

The predicted evolution of the magnitudes in various passbands of CXO 52 is shown in Figure 4. The predicted  $H_{160}$  magnitude at  $z > 6$  is fully consistent with the measured values reported in Bouwens et al. of  $H_{160} = 26.0 - 27.1$ .

### 3.2 Comparison with deep field $i_{775}$ -drops

A search for lower redshift starbursts in the UDF was conducted by Bunker et al. (2004) through the identification

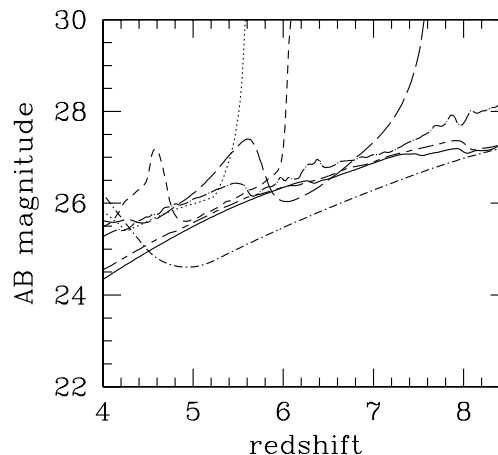


**Figure 4.**  $i_{775}$  (short-dashed line),  $z_{850}$  (long-dashed line),  $J_{110}$  (dotted long-dashed line),  $H_{160}$  (solid line) and  $K_s$  (dotted short-dashed line) AB magnitudes predicted for the Type II QSO CXO 52. Also shown are the predicted magnitudes that would be measured through the  $F070W$  (dotted line) and  $F150W$  (short-dashed long-dashed line) filters by *JWST*. The  $K_s$  magnitude predictions are uncertain for  $z \lesssim 5$  (see text).

of  $i_{775}$ -drops, defined as objects with  $(i_{775} - z_{850})_{AB} > 1.3$ . The method is sensitive to galaxies in the redshift range  $5.8 < z < 7$  through detection of the Ly $\alpha$  break. Follow-up *HST* NICMOS observations were reported by Stanway, McMahon & Bunker (2005). Objects with complete  $i_{775}$ ,  $z_{850}$ ,  $J_{110}$  and  $H_{160}$  photometry are plotted in Figures 5 and 6. Also shown are data from a similar study by Yan & Windhorst (2004). The colour tracks of the various sources considered in this paper are shown for comparison.

The evolution of the predicted  $(i_{775} - z_{850})_{AB}$  colour of the candidate sources is shown in the upper panel of Figure 2. (Not shown are the colours of standard Hubble type galaxies. These are provided by Stanway et al. 2005.) The entrance of the Ly $\alpha$  emission line of the high equivalent width Type II QSO into the  $i_{775}$  passband is visible as a sharp blueing at  $z \gtrsim 4.6$ . This, combined with the rapidly declining flux shortward of restframe  $\lambda < 1400\text{\AA}$ , results in a narrow spur in  $i_{775} - z_{850}$  of redshift width  $\Delta z \approx 0.1$ , as shown in Figures 2 and 5. Although it would seem unlikely to find a Type II QSO in the narrow redshift range near  $z = 4.6$  required for it to be an  $i_{775}$ -drop, it should be borne in mind that the colours are based on a single object. The continuum shape and Ly $\alpha$  emission line strength of a different Type II QSO would in general result in a differently shaped and positioned spur, so that the actual redshift width of Type II QSOs that are  $i_{775}$ -drops may be larger. All the objects, however, will become  $i_{775}$ -dropouts quite abruptly at  $z > 6$  when the Ly $\alpha$  emission line leaves the  $i_{775}$  band, as shown in Figures 2 and 4.

A few of the detected objects in Figures 5 and 6 lie blue-

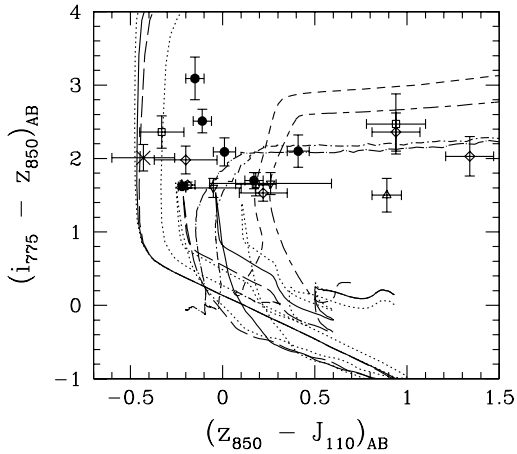


**Figure 5.**  $(i_{775} - z_{850})_{AB}$  vs  $(z_{850} - J_{110})_{AB}$  colour-colour diagram predicted at  $z > 3$  for starburst galaxies of age 30 Myr (dotted long-dashed line) and 600 Myr (dotted short-dashed line), Type I QSO (short-dashed line), and Type II QSO with high equivalent width emission lines (solid line). The dotted lines show the tracks for the Type II QSO with the metal lines boosted or reduced by 50%. The long-dashed line shows the track for the Type II QSO with C IV enhanced by a factor of 2. The short-dashed long-dashed line shows the predictions for a low equivalent width Type II QSO. The locus for the high equivalent width Type II QSO with metal lines cut by 50% lies redward of the solid line in  $(z_{850} - J_{110})_{AB}$  for  $(i_{775} - z_{850})_{AB} < 1.5$ , while the bluest dotted line in  $(z_{850} - J_{110})_{AB}$  corresponds to the Type II QSO with the metals boosted by 50%. The open diamonds and squares and the ‘X’ are from measurements of sources in the UDF by Stanway, McMahon & Bunker (2005). The diamonds are for individual sources, while the squares indicate the composite colours of groups of sources. The ‘X’ shows the colours of stacked source images undetected in  $J_{110}$ . The solid points are from UDF sources identified by Yan & Windhorst (2004). Also shown are the colours of GOODS sources measured by Stanway, Bunker & McMahon (2003) (open triangles) and Eyles et al. (2005) (inverted triangles).

ward in  $(z_{850} - J_{110})_{AB}$  of the expected tracks for starburst galaxies, although reddening of the starburst tracks, which will be stronger in  $(i_{775} - z_{850})_{AB}$  than  $(z_{850} - J_{110})_{AB}$ , may account for part of the discrepancy. Some of these lie near the colour spurs predicted for Type II QSOs at  $z \approx 4.6$ . The corresponding  $(J_{110} - H_{160})$  colours, however, are generally inconsistent with a Type II QSO interpretation.

None the less, several of the source identities have ambiguous interpretations based on colours alone. The three bluest points in  $(z_{850} - J_{110})_{AB}$  from Stanway et al. (2005) shown in Figures 5 and 6 are objects 20104, 25941 and Group 2. None of these readily match the colours of galaxies (although object 25941 is not badly discrepant given its large error bars). The colours of object 20104 are consistent with a Type II QSO with large equivalent width emission lines at  $z = 6.0$ , although the narrow redshift range for

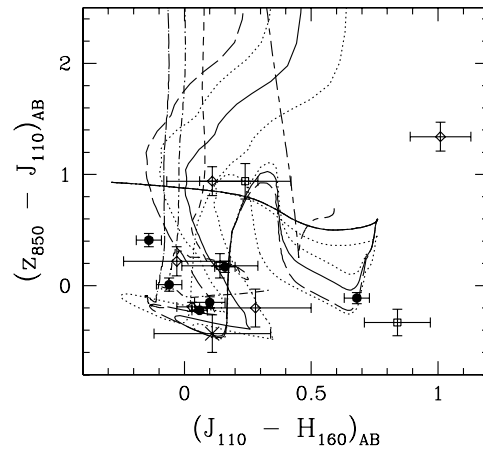


**Figure 6.**  $(z_{850} - J_{110})_{AB}$  vs  $(J_{110} - H_{160})_{AB}$  colour-colour diagram predicted at  $z > 3$  for starburst galaxies of age 30 Myr (dotted long-dashed line) and 600 Myr (dotted short-dashed line), Type I QSO (short-dashed line), and Type II QSO with high equivalent width emission lines (solid line). The dotted lines show the tracks for the Type II QSO with the metal lines boosted or reduced by 50%. The long-dashed line shows the track for the Type II QSO with C IV enhanced by a factor of 2. The short-dashed long-dashed line shows the predictions for a low equivalent width Type II QSO. The locus for the high equivalent width Type II QSO with metal lines boosted by 50% lies blueward of the solid line in  $(J_{110} - H_{160})_{AB}$  for  $(z_{850} - J_{110})_{AB} > 1.1$ . The open diamonds and squares and the ‘X’ are from measurements of sources in the UDF by Stanway, McMahon & Bunker (2005). The diamonds are for individual sources, while the squares indicate the composite colours of groups of sources. The ‘X’ shows the colours of stacked source images undetected in  $J_{110}$ . The solid points are from UDF sources identified by Yan & Windhorst (2004).

$1.3 < (i_{775} - z_{850})_{AB} < 4$  of  $\Delta z \approx 0.1$  (Figure 2) suggests this is unlikely on space density considerations. The same is true of source 25941, with colours marginally matching the colours for a Type II large equivalent width QSO in the narrow  $(i_{775} - z_{850})_{AB}$  spur at  $z = 4.6$ . It also marginally matches the colours for a Type I QSO at  $z \approx 6$ . Additionally, source 23516 matches the colours of a Type I QSO at  $z \approx 5.8$ . The colours of Group 2 have no easy QSO interpretation, nor galactic for that matter; the composite colours appear to be a mix. In addition, the colours of the objects in Group 3 may indicate the group is dominated by a Type I QSO. None of the objects identified by Yan & Windhorst are consistent with the colours expected for QSOs.

An earlier search for  $i_{775}$ -drops was made by Stanway, Bunker & McMahon (2003) using GOODS data, with additional  $i_{775}$ -drops listed in Eyles et al. (2005) accompanied by *Spitzer* data. The reported colours of these sources are plotted in Figure 5. The three points with measured  $(z_{850} - J)_{AB}$  colours all lie near the tips of the spurs for Type II QSOs, and so are equally good matches to Type II QSO

colours as to starburst or Type I QSO colours. From Figure 4,  $(J - K_s)_{AB} \approx 1$  is predicted, in good agreement with the measured values for two of the objects (Eyles et al. ). In these cases, however, follow-up spectroscopy revealed an emission line in each case corresponding to Ly $\alpha$  at  $z \approx 5.8$  (Stanway et al. 2004a,b), so that they are likely not Type II QSOs similar to CXO 52.

They, however, may be low equivalent width Type II QSOs. Particularly interesting is GLARE#3001, which lies directly on the predicted locus for the low equivalent Type II QSO in Figure 5. Assuming the emission line is Ly $\alpha$  at  $z = 5.79$  (Stanway et al. 2004a),  $(i_{775} - z_{850})_{AB} = 1.62$  is predicted, while  $1.66 \pm 0.20$  is measured. Likewise,  $(J - K_s)_{AB} = 1.13$  is predicted while  $0.89 \pm 0.45$  is measured (Eyles et al. ). It should be noted that the absence of a detectable N v  $\lambda 1240$  line does not preclude a Type II QSO, as the Ly $\alpha$  to N v flux ratio can be very large (15–30) in Type II QSOs (Stern et al. 2002; Mainieri 2005). The possible presence of H $\beta$  and O III  $\lambda\lambda 4959, 5008$  would also contribute to the measured Spitzer flux at  $3.6\mu\text{m}$ . This object thus appears a prime candidate for a low equivalent width Type II QSO.

The presence of the  $(i_{775} - z_{850})_{AB} > 1.3$  spurs raises the question of whether some moderate redshift high equivalent width Type II QSOs could masquerade as high redshift starbursts in future surveys. The C IV  $\lambda 1549$  line at  $z = 4.5$  could be mistaken for Ly $\alpha$  at  $z = 6.0$ . Searches for a Balmer break between the  $K_s$  band and  $3.6\mu\text{m}$ , as was done using *Spitzer* data by Eyles et al. , could reveal a false break due to the presence of H $\alpha$  at  $\lambda = 3.6\mu\text{m}$ . The models of Kwan & Krolik predict H $\alpha$  should be 2 – 6 times as strong H $\beta$  , which is a strong line in CXO 52, with about 10% the flux of Ly $\alpha$  (Stern et al. ).

Recently, Malhotra et al. (2005) identified a possible large overdensity of galaxies at  $z = 5.9$  based on slitless low resolution ( $R = 100$ ) grism spectra of *i*-drops in the UDF as part of the GRAPES survey (Pirzkal et al. 2004). The spectra of the 29 sources with  $(i_{775} - z_{850}) > 0.9$  they identify fail to show clear evidence for the presence of any Type II QSOs with strong Ly $\alpha$  emission. One of the sources, object 3317, does however appear to show at least one strong emission line. The source has  $(i_{775} - z_{850}) \approx 1.1 - 1.2$  and lies well away from the predicted colour curves for galaxies (their Figure 2). The grism spectrum for the source (adapted from their Figure 6) is shown in Figure 7 along with their best-fitting model galaxy spectrum. The spectrum of CXO 52, redshifted to  $z = 4.6$ , is also shown, smoothed to  $R = 100$  and rebinned to match the grism spectrum. The emission line at  $\lambda \approx 8600\text{\AA}$  is due to C IV  $\lambda 1549$ . The spectrum was rescaled to give the minimum  $\chi^2$  match to the spectrum, and the effect of intergalactic attenuation was included. A value of  $\chi^2 = 26$  for 27 degrees-of-freedom is found, an improvement over  $\chi^2 = 35$  found for the model galaxy fit. The Ly $\alpha$  emission line has been removed, assuming it has been suppressed, either by dust absorption internal to the galaxy or possibly by damped absorption by a nearby intervening damped Ly $\alpha$  system. (Such  $z_{\text{abs}} \approx z_{\text{em}}$  damped systems are known in absorption line surveys, suggesting the QSO may be part of a galaxy group; eg, Sargent, Boksenberg & Steidel 1988. There is evidence that some low redshift Type II QSOs do reside in groups or clusters; eg, Iwasawa et al. 2005.) The object thus appears a candidate for a Type II QSO.

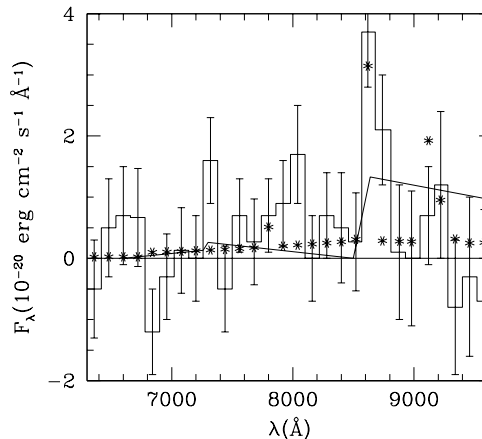


**Figure 7.** A low resolution ( $R = 100$ ) grism spectrum (histogram) of object 3317 in the GRAPES survey from Malhotra et al. (2005), with their best-fitting model galaxy spectrum (solid line). The points show the spectrum of CXO 52, redshifted to  $z = 4.6$  and smoothed and rebinned to the same resolution and sampling as the grism spectrum. The emission line at  $\lambda \approx 8600\text{\AA}$  is due to C IV  $\lambda 1549$ . It is assumed the Ly $\alpha$  emission line has been absorbed (see text).

### 3.3 Predictions for the *James Webb Space Telescope*

The faint magnitude limits that will be achievable by the *James Webb Space Telescope (JWST)* should make possible the detection of substantial numbers of high redshift Type II QSOs, if they are present.

In this section, predictions for the colours detectable by the *JWST* are made. Because the template spectrum does not extend much into the restframe infra-red, the bands considered are restricted to *F070W*, *F110W* and *F150W*. In Figure 8, the  $(m_{070} - J_{110})_{AB}$  vs  $(J_{110} - m_{150})_{AB}$  colours for the Type I and II QSO and starburst spectra are shown. The tracks are not well-separated. Reddening of the starbursts will further compress the tracks in colour-colour space. A much better discriminator is  $(z_{850} - J_{110})_{AB}$  vs  $(J_{110} - m_{150})_{AB}$ , shown in Figure 9. The Type II QSO tracks based on CXO 52 are now well separated from the Type I QSO and starburst tracks. Since the starburst tracks lie redward of the Type II QSO tracks, reddening of the starbursts will not lead to confusion with such Type II QSOs. The predictions for the Type II QSOs are also not very sensitive to the assumed metallicity or C IV to C III ] emission ratio, so that such Type II QSOs should be clearly identifiable once they become  $z_{850}$ -dropouts. The low equivalent width Type II QSO, however, lies near the Type I QSO track and redward of the starburst tracks, so such Type II QSOs would still be difficult to identify uniquely based only on their colours.

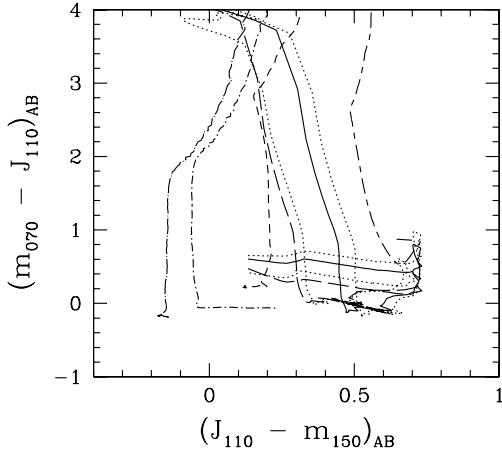


**Figure 8.**  $(m_{070} - J_{110})_{AB}$  vs  $(J_{110} - m_{150})_{AB}$  colour-colour diagram predicted tracks at  $z > 3$  for starburst galaxies of age 30 Myr (dotted long-dashed line) and 600 Myr (dotted short-dashed line), Type I QSO (short-dashed line), and Type II QSO with high equivalent width emission lines (solid line). The dotted lines show the tracks for the Type II QSO with the metal lines boosted or reduced by 50%. The long-dashed line shows the track for the Type II QSO with C IV enhanced by a factor of 2. The short-dashed long-dashed line shows the predictions for a low equivalent width Type II QSO. The tracks all lie near each other. Reddening of the starburst spectra will further compress the locus of tracks.

### 3.4 Predictions for UKIDSS

The UKIRT Infrared Deep Sky Survey (UKIDSS, Lawrence et al. 2005, in preparation) covers the wavelength range  $0.83 - 2.37\mu\text{m}$ , including a new *Y*-band covering  $0.97 - 1.07\mu\text{m}$ , and is expected to continue over the next seven years. The Ultra Deep Survey will reach to (AB)  $K \approx 25$  and  $J \approx 26$  (S. Warren private communication). This is deep enough to detect a source like CXO 52 out to  $z = 5 - 6$  (Figure 4).

The evolution of the colour combinations  $Z - Y$ ,  $Y - J$ ,  $J - H$  and  $H - K$  is shown in Figure 10 for the various sources considered here. Of particular use for identifying Type II QSOs with large equivalent width emission lines are  $Z - Y$  and  $Y - J$ . Type II QSOs in the redshift range  $4.5 < z < 5$  will appear unusually blue in  $Z - Y$ , those in the redshift range  $5 < z < 6$  will appear unusually red in  $Z - Y$ , and those in the redshift range  $6 < z < 7$  will appear unusually blue in  $Z - Y$  and red in  $Y - J$ . Those at  $7 < z < 8$  will appear as  $Z$ -dropouts that are unusually blue in  $Y - J$ , of which those with  $z > 7.5$  will appear unusually red in  $J - H$ . The  $H - K$  colours also suggest lower redshift Type II QSOs may be selected as unusually red for  $3 < z < 4$  and unusually blue for  $4 < z < 4.5$ ; however, as noted above, the  $K$ -band magnitude predictions are very uncertain for  $z \lesssim 5$ .

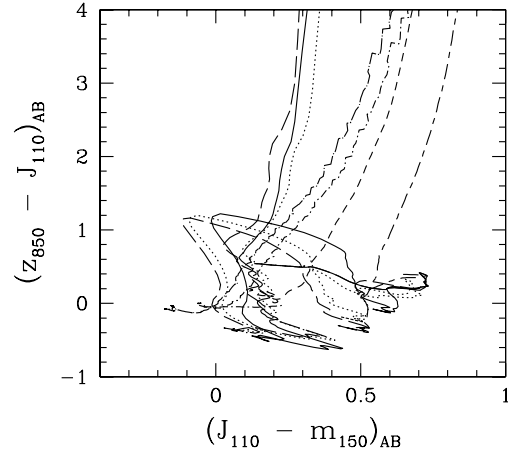


**Figure 9.**  $(z_{850} - J_{110})_{AB}$  vs  $(J_{110} - m_{150})_{AB}$  colour-colour diagram predicted tracks at  $z > 3$  for starburst galaxies of age 30 Myr (dotted long-dashed line) and 600 Myr (dotted short-dashed line), Type I QSO (short-dashed line), and Type II QSO with high equivalent width emission lines (solid line). The dotted lines show the tracks for the Type II QSO with the metal lines boosted or reduced by 50%. The long-dashed line shows the track for the Type II QSO with C IV enhanced by a factor of 2. The short-dashed long-dashed line shows the predictions for a low equivalent width Type II QSO. The high equivalent width Type II QSO track with boosted metals lies blueward of the non-boosted track in  $(J_{110} - m_{150})_{AB}$  for  $(z_{850} - J_{110})_{AB} < 2$  and redward for  $(z_{850} - J_{110})_{AB} > 2$ . The high equivalent width Type II QSO tracks are well separated from the Type I QSO, low equivalent width Type II QSO and starburst tracks.

## 4 SUMMARY AND DISCUSSION

Spectra for Type II QSOs are synthesized based on observed spectra and photometric measurements, and colours predicted at higher redshifts. The possibility that some Type II QSOs have high equivalent widths suggests unusual colours may be expected for these objects, distinct from Type I QSOs and starbursts. It is shown that the colours of the  $z_{850}$ -dropouts discovered in the UDF by Bouwens et al. are matched by Type II QSOs, as are some of the  $i_{775}$ -drops found in the UDF and GOODS. In the case of  $i_{775}$ -drops, the large but measurable  $(i_{775} - z_{850})_{AB}$  colour is achievable in only narrow redshift windows, one at  $z \gtrsim 6$  when the objects abruptly become  $i_{775}$ -dropouts, and a second near  $z = 4.6$  for which  $(i_{775} - z_{850})_{AB} > 1.3$ .

It may seem unlikely to find such objects given their rarity at lower redshifts. It should, however, be noted that even at low redshifts, Type II AGN appear to be a factor of a few to as much as an order of magnitude more abundant than Type I AGNs at low luminosities (Martínez-Sansigre et al. 2005; Simpson 2005). The luminosity function of low-luminosity Type I QSOs at high redshifts is unknown. An estimate is made by Meiksin (2005a), under the assumptions

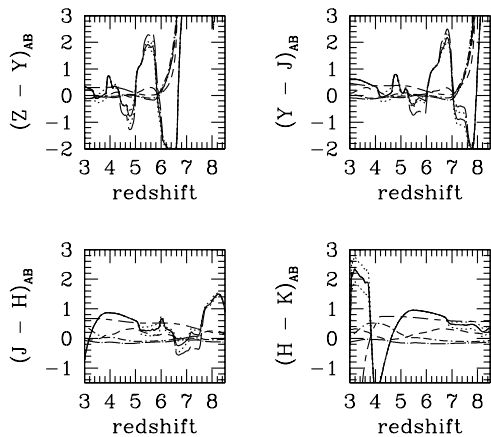


**Figure 10.** Colour evolution of sources in the UKIDSS ZYJHK filter system predicted at  $z > 3$  for starburst galaxies of age 30 Myr (dotted long-dashed line) and 600 Myr (dotted short-dashed line), Type I QSO (short-dashed line), and Type II QSO with high equivalent width emission lines (solid line). The dotted lines show the tracks for the Type II QSO with the metal lines boosted or reduced by 50%. The long-dashed line shows the track for the Type II QSO with C IV enhanced by a factor of 2. The short-dashed long-dashed line shows the predictions for a low equivalent width Type II QSO.

of either pure luminosity evolution (PLE) or pure density evolution (PDE), based on the low luminosity QSO counts of Hunt et al. (2004) at  $z \approx 3$  and the bright QSOs detected at high redshift ( $3.6 \lesssim z \lesssim 6$ ) by the SDSS (Fan et al. 2001, 2004). Using the maximum likelihood PLE model of Meiksin (2005a) (as given in his Table 1), the predicted number of Type I QSOs at  $z > 5.7$  in the  $11.5 \text{ arcmin}^2$  of the UDF with  $z' < 28$  is about 0.07 (0.002 in the PDE model, as the UDF should probe well below the knee in the luminosity function in this model). Thus the number of detectable Type II QSOs in the UDF is expected to lie in the range 0.01 – 1. Within the  $165 \text{ arcmin}^2$  of the GOODS-S ACS field, the number of  $z' < 27$  Type I QSOs at  $z > 5.7$  is predicted in the PLE model to be 0.6 (0.03 in the PDE model), and a number per unit redshift of  $dN/dz \approx 1$  for  $z \approx 4.7$  (0.1 in the PDE model). Thus detecting at least one Type II QSO is possible, although several may be unlikely. But this is one reason why searching for them is of such interest. For instance, if most galaxies went through an AGN phase early in their histories, then, in AGN unification scenarios, most would appear as dim Type II objects. If they went through the AGN phase at  $z \gtrsim 6$ , then their numbers may be larger than the above estimates, and a few to several may be detectable in the UDF and GOODS fields, sufficient to provide a substantial fraction of the photons required to re-ionize the IGM (Meiksin 2005a).

Although the UKIDSS Ultra Deep Survey is a some-

what shallower survey, the relatively large survey area of  $0.78 \text{ deg}^2$  yields a detectable number of Type I QSOs: about six are predicted at  $z > 5.7$  for  $J < 26$  by the PLE model, and  $dN/dz \approx 13$  at  $z \approx 4.7$ . Several Type II QSOs may thus be detectable at these redshifts. While the predicted numbers of Type I QSOs are substantially reduced under the PDE model, about 0.4 at  $z > 5.7$  and  $dN/dz \approx 1.6$  at  $z \approx 4.7$ , the Ultra Deep Survey should prove an effective means for determining which of these models more closely describes the actual evolution of QSOs.

Without follow-up spectroscopy, it is difficult to distinguish a starburst from an AGN. The images of the band-dropout objects tend to be compact (eg, Stanway et al. 2004a), as would be expected for H II regions, but also for an AGN, so images may not readily be used to distinguish starbursts from AGNs. Extended emission would not necessarily preclude an AGN nature either, both because the emitting regions extend from scales of several to a few tens of kiloparsecs in size (Hines et al. 1999) and because some may be embedded in starbursts and so have multiple bright emitting regions; both AGN and starbursts are generally believed to be triggered by merger activity. Even with spectroscopy, high equivalent width Type II QSOs at  $z \approx 4.6$  could still masquerade as starbursts, with C IV emission being mistaken for Ly $\alpha$  at  $z \approx 6.0$ . Strong H $\alpha$  emission, falling at  $\lambda = 3.6 \mu\text{m}$ , could also mimic the  $4000\text{\AA}$  break of a starburst at  $z \approx 6.0$ . Even if Ly $\alpha$  emission is correctly identified, the absence of N V emission does not preclude a Type II QSO, as it would a Type I QSO, since the Ly $\alpha$  to N V ratio in Type II QSOs is observed sometimes to be very large.

The absence of x-ray emission also may not necessarily exclude an AGN nature. The expected x-ray flux appears to cover a broad range for a given UV flux. The ratio of restframe 5.4 keV to  $1915\text{\AA}$  fluxes ( $\nu f_\nu$ ) is 0.45 for CXO 52, and the ratio of restframe 25.7 keV to  $1915\text{\AA}$  fluxes is 4.6 (Stern et al. ). The corresponding values for CDFS-263 are an order of magnitude lower, with a ratio of restframe 5.8 keV to  $1957\text{\AA}$  fluxes of 0.05 and of restframe 27.9 keV to  $1957\text{\AA}$  fluxes of 0.16 (Mainieri et al. ). The 2 Ms deep exposure by *Chandra* has a lower flux limit for the detection of sources of  $1.9 - 9.3 \times 10^{-17} \text{ erg cm}^{-2} \text{ s}^{-1}$  in the 0.5 – 2 keV (soft) band and  $1.1 - 7.5 \times 10^{-16} \text{ erg cm}^{-2} \text{ s}^{-1}$  in the 2 – 8 keV (hard) band, depending on position (Alexander private communication as quoted in Stanway et al. 2004b). At  $z \approx 6$ , this implies a source like CXO 52 would need to have an AB magnitude at  $1.3 \mu\text{m}$  (observed) of about 26.5 – 28 to be detectable in the x-ray, while a source like CDFS-263 would need to be 2.5 or more magnitudes brighter. This is comparable to or somewhat brighter than the *J*- and *H*-band detection limits of the deep surveys used to detect the band-dropout objects.

Although genuine high redshift band-dropout objects are almost certainly dominated by starbursts, the possibility that a few are AGN can have major implications for the re-ionization of the IGM. The potentially important role played by AGNs in re-ionizing the universe may be demonstrated by comparing the numbers of UV ionizing photons generated by black holes and by stars through the lifetime of the universe. The specific luminosity of an AGN at the Lyman edge is  $L_L \simeq 0.1 L_{\text{bol}} / \nu_L$ , where  $L_{\text{bol}}$  is the bolometric luminosity of the AGN and  $\nu_L$  is the frequency of the Lyman edge. The production rate of ionizing photons is then

$\dot{N}_{\text{bh}} \simeq 0.2L_{\text{bol}}/(h\nu_L)$  (Meiksin 2005a), where  $h$  is the Planck constant. Assuming a conversion efficiency  $\epsilon_{\text{bh}}$  of mass into energy for accretion onto a black hole, the global comoving number density of ionizing photons produced by black hole accretion in the universe changes at the rate

$$\dot{n}_{\text{bh}} \simeq \frac{0.2\epsilon_{\text{bh}}\dot{\rho}_{\text{bh}}c^2}{h\nu_L}, \quad (1)$$

where  $\dot{\rho}_{\text{bh}}$  is the rate at which the average comoving mass density of black holes in the universe increases with time (assumed largely due to accretion). The efficiency of mass conversion is unknown, but phenomenological estimates are in the range  $0.1 \lesssim \epsilon_{\text{bh}} \lesssim 0.3$  (eg, Yu & Tremaine 2002).

The production rate of H I ionizing photons by stars is sensitive to the initial mass function (IMF) of the stars and to their metallicities. For a Salpeter IMF with metallicity 20% of solar, the results of Smith, Norris & Crowther (2002) correspond to a production rate of ionizing photons per solar mass of stars formed of  $dN_*/dM \approx 10^{61} \text{ ph M}_{\odot}^{-1}$ . For solar metallicity, the production rate is a factor of 3 smaller, while it may be somewhat larger for Pop III stars. The comoving number density of ionizing photons produced by stars then changes at the rate

$$\dot{n}_* \simeq \frac{dN_*}{dM} \dot{\rho}_*, \quad (2)$$

where  $\dot{\rho}_*$  is the rate at which the average comoving mass density of stars in the universe increases with time.

The number of ionizing photons available to re-ionize the IGM is reduced by internal absorption, both in an AGN and in a star-forming galaxy. Denoting the escape fractions from AGN and galaxies by  $f_{\text{bh,esc}}$  and  $f_{*,\text{esc}}$ , respectively, the ratio of the ionization rate of the IGM by black holes to that by stars is

$$\frac{\dot{n}_{\text{bh}}}{\dot{n}_*} \approx 330 \left( \frac{\epsilon_{\text{bh}}}{0.2} \right) \left( \frac{dN_*/dM}{10^{61} \text{ ph M}_{\odot}^{-1}} \right) \left( \frac{f_{\text{bh,esc}}}{f_{*,\text{esc}}} \right) \left( \frac{\rho_{\text{bh}}}{\rho_*} \right). \quad (3)$$

Here, the approximation is made that  $\dot{\rho}_{\text{bh}}/\dot{\rho}_* \approx \rho_{\text{bh}}/\rho_*$ , averaged over the age of the universe, where  $\rho_{\text{bh}}$  and  $\rho_*$  are the respective mass densities of QSO black holes and in stars in the universe today. This seems a reasonable approximation to make since the inferred growth time of a central massive black hole in a galaxy is comparable to that of the stars in the bulge over a broad range of bulge masses, at least in the present-day universe (Heckman et al. 2004). Estimates for the current mass densities in QSO black holes and stars are  $\rho_{\text{bh}} \approx 10^5 \text{ M}_{\odot} \text{ Mpc}^{-3}$  (Yu & Tremaine 2002) and  $\rho_* \approx 3 \times 10^8 \text{ M}_{\odot} \text{ Mpc}^{-3}$  (Baldry & Glazebrook 2003), both for  $h = 0.7$ . The escape fraction of ionizing photons from AGN is unknown, but their spectra suggest at least half escape, so  $f_{\text{bh,esc}} \approx 0.5$  is assumed. The observational upper limit on the escape fraction of ionizing photons from galaxies is  $f_{*,\text{esc}} < 0.04$  (Fernandez-Soto, Lanzetta & Chen 2002). This then gives for the ratio of IGM ionizing photons produced by black holes to that produced by stars

$$\frac{n_{\text{bh}}}{n_*} \gtrsim \left( \frac{\epsilon_{\text{bh}}}{0.2} \right) \left( \frac{dN_*/dM}{10^{61} \text{ ph M}_{\odot}^{-1}} \right) \left( \frac{f_{\text{bh,esc}}}{0.5} \right) \left( \frac{f_{*,\text{esc}}}{0.04} \right)^{-1}. \quad (4)$$

Despite the low number of black holes compared with stars, their higher mass-to-energy conversion efficiency compared with stellar nuclear fusion and the larger escape fraction from AGN compared with galaxies make black holes compet-

itive with stars as candidate sources for the photons which re-ionized the IGM.

The relative ionization rates may be related to the relative fractions of objects detected in deep surveys as follows. Defining  $f_{\text{AGN}}$  and  $f_{\text{SB}}$  to be the fraction of band-dropout objects that are AGNs and starbursts, respectively,  $f_L/f_M$  the intrinsic ratio of flux densities at the Lyman edge and a fiducial frequency  $\nu_M$  normalising the counts of objects, and  $\alpha_{\text{AGN}}^{\text{eff}}$  and  $\alpha_{\text{SB}}^{\text{eff}}$  the respective effective spectral indices of AGN and starbursts shortward of the Lyman edge, then the ratio of ionizing photon rates of AGN to starbursts injected into the IGM is

$$\frac{\dot{n}_{\text{b}}}{\dot{n}_*} = \frac{f_{\text{AGN}}}{f_{\text{SB}}} \frac{f_{\text{AGN,esc}}}{f_{\text{SB,esc}}} \left( \frac{f_L}{f_M} \right)_{\text{AGN}} \left( \frac{f_L}{f_M} \right)_{\text{SB}}^{-1} \frac{\alpha_{\text{SB}}^{\text{eff}}}{\alpha_{\text{AGN}}^{\text{eff}}}. \quad (5)$$

Here,  $f_{\text{AGN,esc}}$  and  $f_{\text{SB,esc}}$  are the respective escape fractions of ionizing photons from the observed AGN and starbursts. The mean observed AGN escape fraction in particular is expected to be much smaller than the mean black hole escape fraction above because the contribution from Type II AGN is expected to be very small. The only ionizing photons that may be observed from Type II AGN are those re-emitted from the emission line gas illuminated by the central engine: the direct ionizing photons will be obscured. If only Type I AGN are counted in Eq. 5, then  $f_{\text{AGN,esc}}$  may be taken to refer only to these objects, so that  $f_{\text{AGN,esc}} \approx f_{\text{bh,esc}}$ , although it should be noted that the amount of re-radiated ionizing photons from Type II AGN is unknown and may not be completely negligible. It will also be assumed that  $f_{\text{SB,esc}} \approx f_{*,\text{esc}}$ . For Pop III stars and hard spectra AGN,  $\alpha_{\text{SB}}^{\text{eff}} \approx 0.5$  is expected, while for Pop II stars,  $\alpha_{\text{SB}}^{\text{eff}} \approx 1.8 - 2.3$  is expected (Meiksin 2005a), while soft spectra AGN may have  $\alpha_{\text{AGN}}^{\text{eff}} \approx 1.8$ . Further uncertainty arises from the ratio of the flux  $f_L$  at the Lyman limit to the flux  $f_M$  measured most near the Lyman limit. But these likely combine to an uncertainty of a factor of only a few. The dominant uncertainty is  $f_{\text{bh,esc}} f_{\text{AGN}}/f_{*,\text{esc}} f_{\text{SB}}$ . For escape fractions of  $f_{\text{bh,esc}} \approx 0.5$  and  $f_{*,\text{esc}} \approx 0.04$ , only about one object in a dozen, with an uncertainty of a factor of at least a few, need by an AGN for AGN to compete with starbursts as the dominant source of ionizing photons. A further implication of a substantial AGN contribution to the re-ionization of the IGM is that the post-reionization temperature will be substantially boosted if the AGN are sufficiently hard to ionize He II to He III as well, which current AGN number counts suggest they may be able to do by  $z \lesssim 5.5$  (Meiksin 2005a).

Ultimately, combining *HST* observations of  $z_{850}$ -dropouts with future follow-up *JWST* imaging to detect high redshift Type II AGN may be the best means of settling the question of how prevalent Type II QSOs are at high redshifts.

## 5 ACKNOWLEDGEMENTS

The author kindly thanks Steve Warren for providing response curves for the UKIDSS filters and for useful comments, as well as Omar Almaini for helpful comments. The author also thanks the referee Andrew Bunker for several useful comments and suggestions that improved this work.

**REFERENCES**

Antonucci R., 1993, ARAA, 31, 473  
 Baldry I. K., Glazebrook K., 2003, ApJ, 593, 258  
 Bithell M., 1991, MNRAS, 253, 320  
 Bouwens R. J., Thompson R.I., Illingsworth G. D., Franx M., van Dokkum P., Fan X., Dickinson M. E., Eisenstein D. J., Rieke M. J., 2004, ApJ, 616, L79  
 Bunker A. J., Stanway E. R., Ellis R. S., McMahon R. G., 2004, MNRAS, 355, 374  
 Chiu K., Zheng W., Schneider D. P., Glazebrook K., Iye M., Kashikawa N., Tsvetanov Z., Yoshida M., Brinkmann J., 2005, AJ, 130, 13  
 Dawson S., Stern D., Bunker A. J., Spinrad H., Dey A., 2001, AJ, 122, 598  
 Eyles L. P., Bunker A. J., Stanway E. R., Lacy M., Ellis R. S., Doherty M., 2005, MNRAS, in press (astro-ph/0502385)  
 Fan X. et al., 2001, AJ, 121, 54  
 Fan X. et al., 2004, AJ, 128, 515  
 Fernandez-Soto A., Lanzetta K.M., Chen H.-W., 2002, MNRAS, 342, 1215  
 Gandhi P., Crawford C. S., Fabian A. C., Johnstone R. M., 2004, MNRAS, 348, 529  
 Giavalisco M. et al., 2004, ApJ, 600, L103  
 Guhathakurta P., Tyson J. A., Majewski S. R., 1990, ApJ, 357, L9  
 Heckman T. M., Kauffmann G., Brinchmann J., Charlot S., Tremonti C., White S. D. M., 2004, ApJ, 613, 109  
 Hines D. C., Schmidt G. D., Wills B. J., Smith P. S., Sowers L. G., 1999, ApJ, 512, 145  
 Hunt M. P., Steidel C. C., Adelberger K. L., Shapley A. E., 2004, ApJ, 605, 625  
 Iwasawa K., Crawford C. S., Fabian A. C., Wilman R. J., 2005, MNRAS, 362, L20  
 Jarvis M. J., van Breukelen C., Wilman R. J., 2005, MNRAS, 358, L11  
 Kwan J., Krolik J. H., 1981, ApJ, 250, 478  
 Leitherer C. et al., 1999, ApJS, 123, 3  
 Madau P., 1995, ApJ, 441, 18  
 Madau P., Ghisellini G., Fabian A. C., 1994, MNRAS, 270, L17  
 Mainieri V. et al., 2005, MNRAS, 356, 1571  
 Malhotra S. et al., 2005, ApJ, 626, 666  
 Martínez-Sansigre A., Rawlings S., Lacy M., Fadda D., Marleau F. R., Simpson C., Willott C. J., Jarvis M. J., 2005, Nat, 436, 666  
 Meiksin A., 2005a, MNRAS, 356, 596  
 Meiksin A., 2005b, MNRAS, in press  
 Norman C. et al., 2002, ApJ, 571, 218  
 Pirzkal N. et al., 2004, ApJS, 154, 501  
 Sargent W. L. W., Boksenberg A., Steidel C. C., 1988, ApJS, 68, 539  
 Simpson C., 2005, MNRAS, 360, 555  
 Smith L. J., Norris R. P. F., Crowther P. A., 2002, MNRAS, 337, 1309  
 Stanway E. R., Bunker A. J., McMahon R. G., 2003, MNRAS, 342, 439  
 Stanway E. R., McMahon R. G., Bunker A. J., 2005, MNRAS, 359, 1184  
 Stanway E. R. et al., 2004a, ApJ, 604, L13  
 Stanway E. R., Bunker A. J., McMahon R. G., Ellis R. S., Treu T., McCarthy P. J., 2004b, ApJ, 607, 704  
 Steidel C. C., Hamilton D., 1992, AJ, 104, 941  
 Steidel C. C., Hamilton D., 1993, AJ, 105, 2017  
 Steidel C. C., Hunt M. P., Shapley A. E., Adelberger K. L., Pettini M., Dickinson M., Giavalisco M., 2002, ApJ, 576, 653  
 Stern D. et al., 2002, ApJ, 568, 71  
 Stiavelli M., Fall S. M., Panagia N., 2004, ApJ, 610, L1  
 Vanden Berk D. E. et al., 2001, AJ, 122, 549

Yan H., Windhorst R. A., 2004, ApJ, 612, L93  
 Yu Q., Tremaine S., 2002, MNRAS, 335, 965  
 Zakamska N. L. et al., 2003, AJ, 126, 2125